SLAC-PUB-9225
May 2002

Transverse to Longitudinal Emittance Exchange*

M. Cornacchia, P. Emma§
Stanford Linear Accelerator Center, Stanford University, Stanford, CA 94309, USA

Abstract

A scheme is proposed to exchange the transverse and longitudinal emittances of an electron bunch. A general analysis is presented and a specific beamline is used as an example where the emittance exchange is achieved by placing a transverse deflecting mode radio-frequency cavity in a magnetic chicane. In addition to reducing the transverse emittance, the bunch length is also simultaneously compressed. The scheme has the potential to introduce an added flexibility to the control of electron beams and to provide some contingency for the achievement of emittance and peak-current goals in free-electron lasers.

* Work supported by Department of Energy contract number DE-AC03-76SF00515.

§ Electronic address: Emma@SLAC.Stanford.edu

1 Introduction

The main challenge of the Linac Coherent Light Source [1] and other free-electron lasers (FEL) that are currently planned or under design, remains the achievement of a bright electron beam in the transverse plane. Although the FEL also constrains the longitudinal emittance, it appears to be more easily obtainable than that of the transverse plane. In fact, the predictions are that the incoherent momentum spread originating from the photo-injector is too small to effectively damp the micro-bunching instability induced by coherent synchrotron radiation (CSR) [2,3,4]. A motivation therefore exists to reduce the transverse emittance and increase the longitudinal, since this may lead to SASE (self-amplified spontaneous emission) lasing in a shorter undulator length and simultaneously less CSR micro-bunching in the compressor.

We show that, under certain conditions, a transfer of emittance from the transverse to the longitudinal plane (or the reverse) is possible and not impractical. Our implementation uses a radio-frequency cavity in a dispersive region of a four dipole-magnet chicane. The cavity operates in the dipole mode, having a longitudinal electric field with gradient such that its strength varies linearly with transverse distance from the axis. A time dependent magnetic deflecting field is also present. A complete emittance analysis is presented and a specific example is studied.

2 The Dipole-Mode Cavity

Occasionally, an application arises of an RF cavity operating in a dipole mode, where the longitudinal electric field varies linearly with transverse distance from the axis. The earliest mention of such cavities, to the authors' knowledge, appeared in Ref. [5]. The hope of using such cavities to change the damping of the three modes of oscillation of particles in an electron circular accelerator was dashed by Robinson's famous paper [6] that shows that the partition numbers cannot be changed with an RF field. A discussion of the physical mechanism of this general principle as it applies to a dipole mode cavity was presented in Ref. [7]. Cylindrical cavities operating in the TM_{210} mode (thus with a quadratic dependence of the longitudinal electric field on the distance from the axis) to couple the longitudinal and transverse motion to enhance laser cooling of ions in a storage ring [8], or to establish a correlation between betatron amplitude and momentum deviation to condition an FEL electron beam [9], have also been proposed. For the system under consideration we use a rectangular cavity having a longitudinal electric field which varies linearly with transverse distance, x, from the axis, as shown in **Fig. 1**.

In the neighborhood of the axis ($x << a$) we have an accelerating field for an electron crossing the cavity at time t,

$$E_z \approx E_0 \frac{x}{a} \cos(\omega t), \quad E_x = E_y = 0, \tag{1}$$

where z is the longitudinal axis of the reference trajectory, x the horizontal axis, y the vertical, ω the frequency of the cavity oscillations, and a is a constant characteristic of the cavity dimensions. The peak field is $E_0 = V_0/l$, where V_0 is the peak RF voltage and l the cavity length. The vertical motion is neglected in this analysis, since, to first order, no force of the cavity acts in the vertical plane. The associated magnetic field is obtained from Maxwell's equation:

$$\nabla \times \mathbf{E} = -\frac{\partial \mathbf{B}}{\partial t}, \quad B_y \approx \frac{E_0}{a\omega}\sin(\omega t), \quad B_x = B_z = 0\,. \tag{2}$$

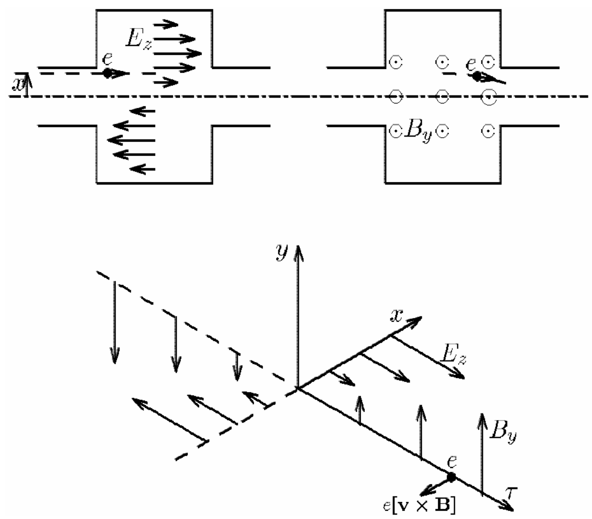

Figure 1. Electric field (top-left) in a dipole-mode cavity at synchronous time (t = 0), and the magnetic field (top-right) one-quarter oscillation later. Longitudinal electric and vertical magnetic fields around t = 0 (bottom).

The small relative energy change, $\delta\ (\equiv \Delta\gamma/\gamma << 1)$, of an electron traversing the cavity at a distance x from the axis is

$$\delta \approx \frac{eV_0}{E}\frac{x}{a}\cos(\omega t), \tag{3}$$

where E is the nominal electron energy. We phase the cavity such that the center of the bunch (the reference particle) passes through the cavity at time t = 0, when the electric field gradient is at its maximum and the magnetic field passes through zero. We consider a bunch length that is much smaller than the RF wavelength (*i.e.*, $|\omega t| << 1$). Thus, to first order,

$$\delta \approx \frac{eV_0}{E}\frac{x}{a} = kx, \qquad k \equiv \frac{eV_0}{aE}\,. \tag{4}$$

The horizontal deflection angle due to the vertical magnetic field of the cavity is

$$\Delta x' \approx \frac{eV_0}{E}\frac{ct}{a} = kct \approx kz\,, \tag{5}$$

and z is the longitudinal distance from the center of this ultra-relativistic bunch.

3 Emittance Exchange

We now analyze the emittance exchange concept and return to the cavity implementation later. The following is a general 4-dimensional linear beam transport analysis [10] in the *x*-*z* plane (or *x*-*y* plane). The initial uncoupled 4×4 beam covariance matrix, σ_0, can be written as [11]

$$\boldsymbol{\sigma}_0 = \begin{bmatrix} \varepsilon_{x_0}\beta_x & -\varepsilon_{x_0}\alpha_x & 0 & 0 \\ -\varepsilon_{x_0}\alpha_x & \varepsilon_{x_0}\gamma_x & 0 & 0 \\ 0 & 0 & \varepsilon_{z_0}\beta_z & -\varepsilon_{z_0}\alpha_z \\ 0 & 0 & -\varepsilon_{z_0}\alpha_z & \varepsilon_{z_0}\gamma_z \end{bmatrix} = \begin{bmatrix} \boldsymbol{\sigma}_x & \mathbf{0} \\ \mathbf{0} & \boldsymbol{\sigma}_z \end{bmatrix}, \tag{6}$$

where $\alpha_{x,z}$, $\beta_{x,z}$, and $\gamma_{x,z}$ ($\equiv \{1+\alpha_{x,z}{}^2\}/\beta_{x,z}$) are the beam envelope functions, and ε_{x_0} and ε_{z_0} are the initial uncoupled beam emittances in the horizontal and longitudinal planes. The rms beam sizes (horizontal and longitudinal) are related to the respective rms emittances by the relations

$$\sigma_x = \sqrt{\varepsilon_{x_0}\beta_x}\,,\ \sigma_z = \sqrt{\varepsilon_{z_0}\beta_z}\ . \tag{7}$$

The bunch 'chirp', or linear energy slope along the bunch length, is related to the longitudinal parameters by

$$\frac{\langle z\delta\rangle}{\sigma_z^2} = -\frac{\alpha_z}{\beta_z}, \tag{8}$$

with the total rms relative energy spread, σ_δ, given by

$$\sigma_\delta = \sqrt{\varepsilon_{z_0}(1+\alpha_z^2)/\beta_z} = \sqrt{\sigma_{\delta_u}{}^2 + \sigma_{\delta_c}{}^2}\ . \tag{9}$$

Here σ_{δ_u} and σ_{δ_c} are the time-uncorrelated and time-correlated relative energy spread components, respectively, which add in quadrature. The normalized longitudinal emittance is

$$\gamma\varepsilon_z = \gamma\sqrt{\sigma_z^2\sigma_\delta^2 - \langle z\delta\rangle^2}\,, \tag{10}$$

with $\gamma\,(= E/mc^2)$ the beam energy in units of electron rest mass. In the simple case, with no time-correlated energy spread (*i.e.*, $\langle z\delta\rangle = 0$), the longitudinal emittance is

$$\gamma\varepsilon_z(\alpha_z = 0) = \gamma\sigma_z\sigma_\delta = \sigma_z\frac{\sigma_E}{mc^2}, \tag{11}$$

where σ_E is the absolute rms energy spread. Now propagate the beam through a 4×4 beamline transfer matrix, **R**, starting from an initial beam σ_0, with $\mathbf{R}^T$ as the transpose of the matrix **R**.

$$\boldsymbol{\sigma} = \mathbf{R}\boldsymbol{\sigma}_0\mathbf{R}^T \tag{12}$$

Since **R** is symplectic and therefore $\det(\mathbf{R}) \equiv |\mathbf{R}| = 1$, the 4-D emittance ($= \varepsilon_{x_0}\varepsilon_{z_0}$) of σ_0 is unchanged by **R**. The 4×4 matrix **R** is constructed from four 2×2 blocks, **A**, **B**, **C**, and **D** [12], as

$$\mathbf{R} = \begin{bmatrix} \mathbf{A} & \mathbf{B} \\ \mathbf{C} & \mathbf{D} \end{bmatrix}, \tag{13}$$

with

$$\mathbf{A} = \begin{pmatrix} a_{11} & a_{12} \\ a_{21} & a_{22} \end{pmatrix}, \quad \mathbf{B} = \begin{pmatrix} b_{11} & b_{12} \\ b_{21} & b_{22} \end{pmatrix}, \quad etc., \tag{14}$$

and it follows from (12) that the new beam, after beamline **R**, is

$$\boldsymbol{\sigma} = \begin{pmatrix} \mathbf{A}\boldsymbol{\sigma}_x\mathbf{A}^T + \mathbf{B}\boldsymbol{\sigma}_z\mathbf{B}^T & \mathbf{A}\boldsymbol{\sigma}_x\mathbf{C}^T + \mathbf{B}\boldsymbol{\sigma}_z\mathbf{D}^T \\ \mathbf{C}\boldsymbol{\sigma}_x\mathbf{A}^T + \mathbf{D}\boldsymbol{\sigma}_z\mathbf{B}^T & \mathbf{C}\boldsymbol{\sigma}_x\mathbf{C}^T + \mathbf{D}\boldsymbol{\sigma}_z\mathbf{D}^T \end{pmatrix}, \tag{15}$$

with σ_x and σ_z the 2×2 block matrices of the x and z planes as shown in (6). The squares of the projected rms x and z emittances are the determinants of the 2×2 on-diagonal blocks.

$$\begin{aligned} \varepsilon_x^2 &= \left|\mathbf{A}\boldsymbol{\sigma}_x\mathbf{A}^T + \mathbf{B}\boldsymbol{\sigma}_z\mathbf{B}^T\right| \\ \varepsilon_z^2 &= \left|\mathbf{C}\boldsymbol{\sigma}_x\mathbf{C}^T + \mathbf{D}\boldsymbol{\sigma}_z\mathbf{D}^T\right| \end{aligned} \tag{16}$$

We recall that the determinant of the sum of 2×2 matrices can be expressed using the trace (tr) as

$$\left|\mathbf{X} + \mathbf{Y}\right| = \left|\mathbf{X}\right| + \left|\mathbf{Y}\right| + tr\left\{\mathbf{X}^a\mathbf{Y}\right\}, \tag{17}$$

where $\mathbf{X}^a$ is the adjoint of **X** (used here to avoid inverting **A**, **B**, **C**, or **D** which may be singular).

$$\mathbf{X}^a = \left|\mathbf{X}\right|\mathbf{X}^{-1}, \ \left|\mathbf{X}\right| \neq 0, \quad \text{or} \quad \mathbf{X}^a = \mathbf{J}^{-1}\mathbf{X}^T\mathbf{J}, \quad \text{with } \mathbf{J} \equiv \begin{pmatrix} 0 & 1 \\ -1 & 0 \end{pmatrix}, \quad \mathbf{J}^2 = -\mathbf{I}. \tag{18}$$

Applying the above matrix property, (16) becomes

$$\begin{aligned} \varepsilon_x^2 &= \left|\mathbf{A}\right|^2 \varepsilon_{x_0}^2 + \left|\mathbf{B}\right|^2 \varepsilon_{z_0}^2 + tr\left\{\left(\mathbf{A}\boldsymbol{\sigma}_x\mathbf{A}^T\right)^a \mathbf{B}\boldsymbol{\sigma}_z\mathbf{B}^T\right\}, \\ \varepsilon_z^2 &= \left|\mathbf{C}\right|^2 \varepsilon_{x_0}^2 + \left|\mathbf{D}\right|^2 \varepsilon_{z_0}^2 + tr\left\{\left(\mathbf{C}\boldsymbol{\sigma}_x\mathbf{C}^T\right)^a \mathbf{D}\boldsymbol{\sigma}_z\mathbf{D}^T\right\}, \end{aligned} \tag{19}$$

where |**A**|, |**B**|, |**C**|, and |**D**|, are the determinants of the 2×2 blocks of the net transfer matrix **R**.

Using an alternate form for the initial uncoupled beam, σ_x and σ_z,

$$\begin{aligned} \boldsymbol{\sigma}_x &= \varepsilon_{x_0}\mathbf{Q}_x\mathbf{Q}_x^T, \qquad \mathbf{Q}_x \equiv \frac{1}{\sqrt{\beta_x}}\begin{pmatrix} \beta_x & 0 \\ -\alpha_x & 1 \end{pmatrix}, \\ \boldsymbol{\sigma}_z &= \varepsilon_{z_0}\mathbf{Q}_z\mathbf{Q}_z^T, \qquad \mathbf{Q}_z \equiv \frac{1}{\sqrt{\beta_z}}\begin{pmatrix} \beta_z & 0 \\ -\alpha_z & 1 \end{pmatrix}, \end{aligned} \tag{20}$$

and the property of the trace: $tr\{\mathbf{XYZ}\} = tr\{\mathbf{YZX}\} = tr\{\mathbf{ZXY}\}$, we obtain, from (19)

$$\varepsilon_x^2 = |\mathbf{A}|^2 \varepsilon_{x_0}^2 + |\mathbf{B}|^2 \varepsilon_{z_0}^2 + \varepsilon_{x_0} \varepsilon_{z_0} tr\left\{\mathbf{U}\mathbf{U}^T\right\},$$
$$\varepsilon_z^2 = |\mathbf{C}|^2 \varepsilon_{x_0}^2 + |\mathbf{D}|^2 \varepsilon_{z_0}^2 + \varepsilon_{x_0} \varepsilon_{z_0} tr\left\{\mathbf{V}\mathbf{V}^T\right\}, \quad (21)$$

where

$$\mathbf{U} \equiv \mathbf{Q}_x^{-1} \mathbf{A}^a \mathbf{B} \mathbf{Q}_z,$$
$$\mathbf{V} \equiv \mathbf{Q}_x^{-1} \mathbf{C}^a \mathbf{D} \mathbf{Q}_z. \quad (22)$$

We now use the symplectic condition with **S** [13] as the 4×4 form of **J**,

$$\mathbf{R}^T \mathbf{S} \mathbf{R} = \mathbf{R} \mathbf{S} \mathbf{R}^T = \mathbf{S} = \begin{pmatrix} \mathbf{J} & \mathbf{0} \\ \mathbf{0} & \mathbf{J} \end{pmatrix}, \quad (23)$$

which gives a relation between the submatrices

$$\left|\mathbf{A}^T \mathbf{J} \mathbf{A} + \mathbf{C}^T \mathbf{J} \mathbf{C}\right| = \left|\mathbf{A} \mathbf{J} \mathbf{A}^T + \mathbf{B} \mathbf{J} \mathbf{B}^T\right| = 1,$$
$$\left|\mathbf{B}^T \mathbf{J} \mathbf{B} + \mathbf{D}^T \mathbf{J} \mathbf{D}\right| = \left|\mathbf{C} \mathbf{J} \mathbf{C}^T + \mathbf{D} \mathbf{J} \mathbf{D}^T\right| = 1, \quad (24)$$

and find the following relations between the sub-matrix determinants

$$|\mathbf{A}| + |\mathbf{C}| = 1, \qquad |\mathbf{A}| = |\mathbf{D}|, \qquad |\mathbf{B}| = |\mathbf{C}|. \quad (25)$$

The **U** and **V** matrices of (22) are shown to be related by using

$$\mathbf{V} = \mathbf{Q}_x^{-1} \mathbf{C}^a \mathbf{D} \mathbf{Q}_z = \mathbf{Q}_x^{-1} \left(\mathbf{J}^{-1} \mathbf{C}^T \mathbf{J}\right) \mathbf{D} \mathbf{Q}_z, \quad (26)$$

and from the off-diagonal 2×2 block of (23), $\mathbf{C}^T\mathbf{J}\mathbf{D} = -\mathbf{A}^T \mathbf{J}\mathbf{B}$, so that

$$\mathbf{V} = \mathbf{Q}_x^{-1} \mathbf{J}^{-1} \left(\mathbf{C}^T \mathbf{J} \mathbf{D}\right) \mathbf{Q}_z = \mathbf{Q}_x^{-1} \mathbf{J}^{-1} (-\mathbf{A}^T \mathbf{J} \mathbf{B}) \mathbf{Q}_z = -\mathbf{Q}_x^{-1} \mathbf{A}^a \mathbf{B} \mathbf{Q}_z = -\mathbf{U}, \quad (27)$$

and therefore

$$tr\left\{\mathbf{U}\mathbf{U}^T\right\} = tr\left\{\mathbf{V}\mathbf{V}^T\right\}, \quad (28)$$

which is simply the sum of the squares of the normalized coupling block of the transfer matrix, and is positive.

$$tr\left\{\mathbf{U}\mathbf{U}^T\right\} = U_{11}^2 + U_{12}^2 + U_{21}^2 + U_{22}^2 \equiv \lambda^2 \geq 0 \quad (29)$$

The emittances at the exit of the beamline are now related to the emittances at the start of the beamline (subscript "0") by

$$\varepsilon_x^2 = |\mathbf{A}|^2 \varepsilon_{x_0}^2 + (1-|\mathbf{A}|)^2 \varepsilon_{z_0}^2 + \varepsilon_{x_0}\varepsilon_{z_0}\lambda^2,$$
$$\varepsilon_z^2 = (1-|\mathbf{A}|)^2 \varepsilon_{x_0}^2 + |\mathbf{A}|^2 \varepsilon_{z_0}^2 + \varepsilon_{x_0}\varepsilon_{z_0}\lambda^2. \tag{30}$$

From (30), if $\varepsilon_{x_0} = \varepsilon_{z_0}$, then $\varepsilon_x = \varepsilon_z$. That is, equal initial *uncoupled* emittances will always remain equal through a symplectic map. Additionally, if λ^2 is insignificant, which it can be, then setting $|\mathbf{A}| = 0$ will produce a complete *x*- to *z*-plane emittance exchange. Note that $\lambda^2 \neq 0$ unless all $A_{ij} = 0$, or the trivial case of no coupling at all, where all $B_{ij} = C_{ij} = 0$.

4 An Emittance Exchanger Beamline

We then apply this derivation to the chicane and dipole-mode cavity system shown in **Fig. 2**. A magnetic chicane sets up a dispersive region at its center, where the cavity is located. The chicane, of full length *L*, is made of four bending magnets and no quadrupole magnets.

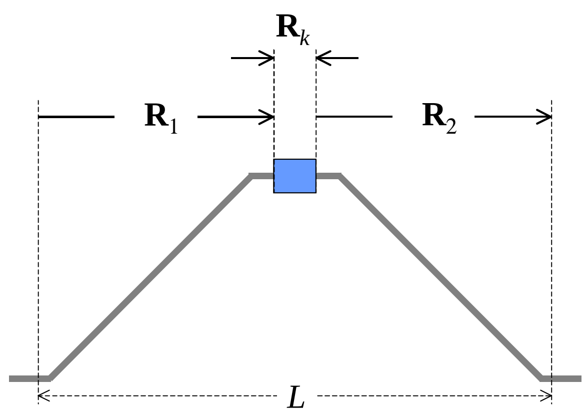

Figure 2. **Schematic diagram of the chicane and transverse cavity.**

From (4) and (5), the transfer matrix of the 'thin-lens' cavity is

$$\mathbf{R}_k = \begin{bmatrix} 1 & 0 & 0 & 0 \\ 0 & 1 & k & 0 \\ 0 & 0 & 1 & 0 \\ k & 0 & 0 & 1 \end{bmatrix}, \tag{31}$$

which is similar to a thin-lens skew quadrupole transfer matrix, but in x, x', z, δ space, rather than x, x', y, y' space. (The effects of a thick-lens are discussed in section **6**.) The transfer matrix across the entire chicane is

$$\mathbf{R} = \mathbf{R}_2 \mathbf{R}_k \mathbf{R}_1, \tag{32}$$

where $\mathbf{R}_1$ and $\mathbf{R}_2$ are the transfer matrices of the first and second section of the chicane, respectively (see **Fig. 2**), and ξ is the momentum compaction ($\xi \equiv R_{56}$) of the full chicane ($\xi > 0$ for chosen coordinates with bunch head at $z > 0$).

$$\mathbf{R}_1=\begin{bmatrix}1 & L/2 & 0 & \eta\\ 0 & 1 & 0 & 0\\ 0 & \eta & 1 & \xi/2\\ 0 & 0 & 0 & 1\end{bmatrix},\qquad \mathbf{R}_2=\begin{bmatrix}1 & L/2 & 0 & -\eta\\ 0 & 1 & 0 & 0\\ 0 & -\eta & 1 & \xi/2\\ 0 & 0 & 0 & 1\end{bmatrix} \tag{33}$$

The matrix of the full chicane and cavity system is

$$\mathbf{R}=\begin{bmatrix}1-\eta k & L & kL/2 & k\left(\frac{\xi L}{4}-\eta^2\right)\\ 0 & 1+\eta k & k & k\xi/2\\ k\xi/2 & k\left(\frac{\xi L}{4}-\eta^2\right) & 1-\eta k & \xi\\ k & kL/2 & 0 & 1+\eta k\end{bmatrix}, \tag{34}$$

$$|\mathbf{A}|=|\mathbf{D}|=1-\eta^2k^2,\qquad |\mathbf{B}|=|\mathbf{C}|=\eta^2k^2 \tag{35}$$

The expression for λ^2 has four terms and is quite long and awkward, even for this system.

$$\mathbf{U}=\mathbf{Q}_x^{-1}\mathbf{A}^a\mathbf{B}\mathbf{Q}_z^{-1} \tag{36}$$

$$\lambda^2=tr\left\{\mathbf{U}\mathbf{U}^T\right\}\Rightarrow 4\text{ terms}$$

A simpler form of λ^2 is easily written by assuming ηk = 1 (*i.e.*, $|\mathbf{A}|$ = 0).

$$\lambda^2=\frac{4\left(1+\alpha_x^2\right)\left(1+\alpha_z^2\right)}{k^2\beta_x\beta_z}=\frac{4\sigma_{x'}^2\sigma_\delta^2\eta^2}{\varepsilon_{x_0}\varepsilon_{z_0}} \tag{37}$$

Thus the emittances at the end of the chicane can be exchanged up to a cross term which is related to the rms divergence, $\sigma_{x'}$, and energy spread, σ_δ, of the initial beam, or

$$\begin{aligned}\varepsilon_x&=\varepsilon_{z_0}\sqrt{1+\frac{4\left(1+\alpha_x^2\right)\left(1+\alpha_z^2\right)}{k^2\beta_x\beta_z}\left(\frac{\varepsilon_{x_0}}{\varepsilon_{z_0}}\right)}=\sqrt{\varepsilon_{z_0}^2+4\sigma_{x'}^2\sigma_\delta^2\eta^2}>\varepsilon_{z_0},\\ \varepsilon_z&=\varepsilon_{x_0}\sqrt{1+\frac{4\left(1+\alpha_x^2\right)\left(1+\alpha_z^2\right)}{k^2\beta_x\beta_z}\left(\frac{\varepsilon_{z_0}}{\varepsilon_{x_0}}\right)}=\sqrt{\varepsilon_{x_0}^2+4\sigma_{x'}^2\sigma_\delta^2\eta^2}>\varepsilon_{x_0}.\end{aligned} \tag{38}$$

It should be recalled that the parameters, $\beta_{x,z}$, $\alpha_{x,z}$, ε_{x_0,z_0}, $\sigma_{x'}$, and σ_δ, all describe the beam at entrance to the chicane. As demonstrated in the example below, the cross-term coefficient, λ^2, can be made insignificantly small for reasonable beam parameters allowing almost complete emittance exchange.

5 Numerical Example

For an example, we take for the four-dipole chicane shown in **Fig. 2** with an X-band RF deflecting cavity ($\omega/2\pi \approx 11.4$ GHz. $a \approx 1.3$ cm) at its center. The beamline and beam parameters at the start of the chicane are listed in **Table 1**. Here we use $\varepsilon_{x_0} > \varepsilon_{z_0}$, which is a required condition for the reduction of the transverse emittance, and one which may not be trivially realized. With these parameters used in (38), we have

$$\begin{aligned} \gamma\varepsilon_{x_0} &= 5\ \mu\text{m} \rightarrow \quad \gamma\varepsilon_x = \gamma\varepsilon_{z_0}\sqrt{1+0.014} \approx 1\ \mu\text{m}, \\ \gamma\varepsilon_{z_0} &= 1\ \mu\text{m} \rightarrow \quad \gamma\varepsilon_z = \gamma\varepsilon_{x_0}\sqrt{1+0.003} \approx 5\ \mu\text{m}, \end{aligned} \tag{39}$$

and have completely exchanged the emittance levels. These results are verified with the computer tracking code *TURTLE* [14] up to 2$^{\text{nd}}$-order. The tracking output is shown in **Fig. 3**.

Table 1. Beam and system parameters as an example for emittance exchange.

Parameter	**symbol**	**value**	**unit**
Initial horizontal normalized emittance	$\gamma\varepsilon_{x_0}$	5	μm
Initial longitudinal normalized emittance	$\gamma\varepsilon_{z_0}$	1	μm
Initial horizontal beta-function	β_x	2.6	m
Initial longitudinal beta-function	β_z	2.9	m
Initial horizontal alpha-function	α_x	0	
Initial longitudinal alpha-function	α_z	0	
Initial rms bunch length	σ_z	100	μm
Initial rms relative energy spread	σ_δ	3.4	10^{-5}
Electron energy	E	150	MeV
Momentum compaction of chicane (R_{56})	ξ	17.7	mm
Full length of chicane	L	2.6	m
Bend angle of each chicane dipole	$\|\theta\|$	5.2	deg
Horizontal dispersion in center of chicane	η	100	mm
Transverse cavity strength parameter	k	10	m^{-1}
Peak RF voltage on crest phase	V_0	20	MV
Cavity dimension	a	1.3	cm
Cavity RF frequency	$\omega/2\pi$	11.4	GHz

The system described here, with $k = 1/\eta$, leaves the x and z planes insignificantly correlated (*i.e.*, $\langle xz\rangle \approx 0$, $\langle x\delta\rangle \approx 0$, $\langle x'z\rangle \approx 0$, $\langle x'\delta\rangle \approx 0$). Note that the bunch length is also compressed by a factor of five at chicane exit ($\sigma_z = 100\ \mu\text{m} \rightarrow 19\ \mu\text{m}$), which is a very desirable feature for an FEL requiring a high peak current. The final bunch length, σ_{z_f}, and energy spread, σ_{δ_f}, for $k = 1/\eta$, and $\alpha_x = \alpha_z = 0$ are

$$\sigma_{z_f}^2 = k^2\varepsilon_{x_0}\left[\frac{\xi^2\beta_x}{4} + \frac{1}{\beta_x}\left(\frac{\xi L}{4} - \frac{1}{k^2}\right)^2\right] + \xi^2\sigma_\delta^2, \tag{40}$$

$$\sigma_{\delta_f}^2 = k^2\varepsilon_{x_0}\left[\beta_x + \frac{L^2}{4\beta_x}\right] + 4\sigma_\delta^2. \tag{41}$$

The energy spread has also increased to 0.24%, a level that is sensitive to the choice of η (= $1/k$) and also β_x at chicane entrance. In addition, the final β_x and α_x functions are greatly magnified by the transverse deflecting field (in this case: β_x = 2.6 m $\to$ 520 m, α_x = 0 $\to$ –400).

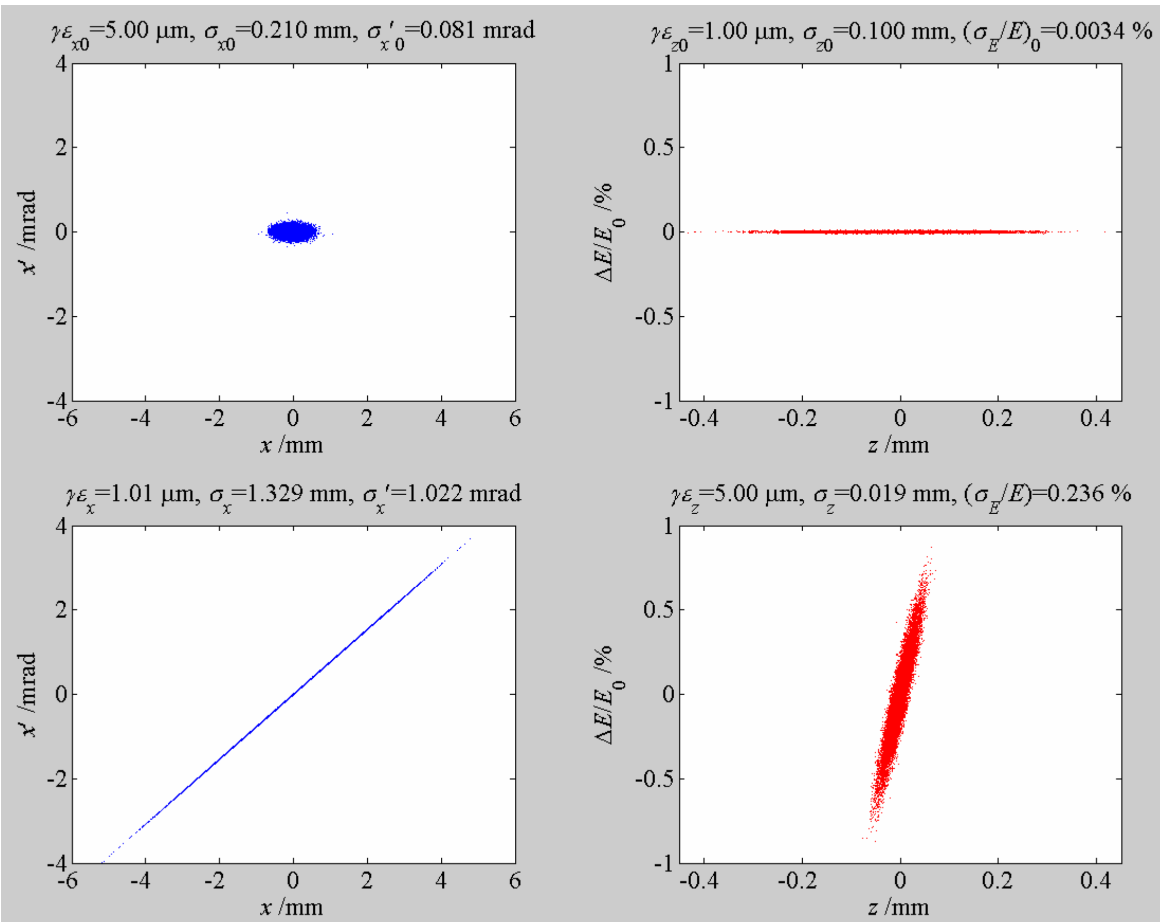

Figure 3. Initial (top) and final (bottom) phase space tracking plots. The horizontal and longitudinal emittances are completely exchanged, as predicted by (38).

In this example the initial energy-time correlation, α_z, was set to zero. In fact a reasonable tolerance on this condition is acceptable. If the initial energy spread is ~3-times larger due to a linear time-correlation ($\alpha_z \approx 2.6$), the final horizontal emittance is increased by ~10% in this case, as given by (38). A non-linear initial energy-time correlation, such as induced by space-charge forces or longitudinal wakefields prior to the chicane, will generate a non-linear position-angle correlation in transverse phase space after the chicane. The longitudinal and transverse emittances, ε_{x_0} and ε_{z_0}, should therefore be considered as projected emittances, which may be increased by non-linear correlations with their conjugate variables. This presents a practical limitation for the exchange process, where the initial beam may need to be cleaned of aberrations prior to emittance exchange.

Finally, the exchanger beamline has some strange properties, which may be surprising on first observation. For example, betatron centroid oscillations initiated prior to the chicane will nearly disappear after the chicane (when scaled to local beam size), instead generating energy and timing shifts to the electron bunch ($\langle x_0\rangle = 1\cdot\sigma_x \;\rightarrow\; \langle z\rangle \approx 1\cdot\sigma_z$). On the other hand, bunch arrival time variations upstream of the chicane will not change the bunch arrival time after the chicane, instead generating betatron oscillations in the horizontal plane. This may be an advantage over standard compressors since it effectively absorbs electron gun-timing variations and keeps them from becoming final bunch length and final energy jitter. This behavior is evident in (34) with $\eta k = 1$.

6 Thick-Lens and Second-Order Effects

Second-order optical aberrations can become significant, due mostly to the second-order dispersion from cavity to end of chicane, if the final energy spread becomes too large. This can be controlled by decreasing the initial beta function, β_x, or increasing the chicane dispersion, η (which reduces the cavity voltage). The relative emittance increase above the linear calculation of (38), which is due to second-order dispersion, is approximately given by

$$\frac{\varepsilon_{x_2}}{\varepsilon_x} \approx \sqrt{1+2\left(\frac{\sigma_z\beta_x}{\eta^2}\frac{\varepsilon_{x_0}}{\varepsilon_{z_0}}\right)^2}\,, \tag{42}$$

where σ_z and β_x are the initial beam parameters at chicane entrance. In the above case, second-order aberrations are insignificant, but a choice of $\eta = 50$ mm (rather than 100 mm) and $\beta_x = 10$ m (rather than 2.6 m) causes a factor of three final horizontal emittance increase above the linear expectations of (38), and a final rms energy spread of 0.8% (rather than 0.2%). This has been verified using *TURTLE* tracking. The values for β_x and η should be chosen carefully with (42) as a guide.

The emittance exchanger beamline described above uses a thin-lens model of a transverse deflecting RF cavity to demonstrate the concept. Of course, the cavity will have some length, especially to produce many mega-volts. A modification of (31), (34), (37), and (38) is necessary to include this. The matrix of the thick-lens transverse cavity is

$$\mathbf{R}_k = \begin{bmatrix} 1 & l & kl/2 & 0 \\ 0 & 1 & k & 0 \\ 0 & 0 & 1 & 0 \\ k & kl/2 & k^2l/6 & 1 \end{bmatrix}, \tag{43}$$

where l is the cavity length. Using this in (32), and continuing with the case $\eta k = 1$, produces a modified **R** with **A** and **B** blocks which are then used in (36) to calculate λ^2.

$$\lambda^2 = \frac{\left(1+\alpha_x^2\right)\left\{576+48k^2l\xi-4k^2l\alpha_z\beta_z\left(24+k^2l\xi\right)+\alpha_z^2\left(24+k^2l\xi\right)^2+k^4l^2\left(4\beta_z^2+\xi^2\right)\right\}}{144k^2\beta_x\beta_z} \tag{44}$$

With $l = 0$ this reduces to (37), but otherwise can be a much more significant limitation in the emittance exchange. If this is now minimized with respect to α_z, it becomes

$$\lambda_{min}^2 = \frac{4\left(1+\alpha_x^2\right)\left(1+k^2l\xi/24\right)^2}{k^2\beta_x\beta_z}, \tag{45}$$

at a value of α_z (related by (8) to the initial energy-time chirp in the bunch), which is given by

$$\alpha_{z_{min}} = \frac{1}{12}\left(\frac{k^2l\beta_z}{1+k^2l\xi/24}\right). \tag{46}$$

The expression for λ^2 in (45) will reduce to that of (37) with $\alpha_z = 0$ if $k^2l\xi/24 << 1$. For an X-band cavity with ~50 MV/m, the level of 20 MV is achieved with $l = 0.4$ m. From **Table 1**, the values of k and ξ give $k^2l\xi/24 \approx 0.03$. Therefore, the emittance exchanger for a thick-lens works almost exactly like the thin-lens as long as α_z (*i.e.*, the incoming energy chirp) is given by (46) (*i.e.*, $\alpha_z \approx 9.4$ in this case). From (9), this means an initial correlated energy spread of 0.03%.

Particle tracking is repeated in Fig. 4 with a thick-lens cavity ($l = 0.4$ m) and α_z set according to (46). The initial energy chirp is evident in the upper right plot. The emittances are again completely exchanged in this more general, and more realistic case. The emittance exchange relations of (38) are now modified for the thick-lens case ($l \neq 0$), and are given (with $\eta k = 1$) by,

$$\begin{aligned} \varepsilon_x &= \varepsilon_{z_0}\sqrt{1+\frac{4\left(1+\alpha_x^2\right)\left(1+k^2l\xi/24\right)^2}{k^2\beta_x\beta_z}\left(\frac{\varepsilon_{x_0}}{\varepsilon_{z_0}}\right)} > \varepsilon_{z_0}, \\ \varepsilon_z &= \varepsilon_{x_0}\sqrt{1+\frac{4\left(1+\alpha_x^2\right)\left(1+k^2l\xi/24\right)^2}{k^2\beta_x\beta_z}\left(\frac{\varepsilon_{z_0}}{\varepsilon_{x_0}}\right)} > \varepsilon_{x_0}. \end{aligned} \tag{47}$$

In (47), the initial energy chirp, α_z, is not a free parameter and must follow (46). Otherwise (44) must be substituted into (30) for the more general case. Note in (30) that if $\eta k \neq 1$ and $k \neq 0$, both 'projected' emittances can simultaneously increase to very large levels, both much larger than the largest initial emittance. This is because the beams become highly coupled in this case and the single-plane *projected* emittances do not reflect the *intrinsic* beam emittances, but are simply the quantities measured in those particular planes. The full 4D phase space volume is, of course, preserved since always $|\mathbf{R}| = 1$.

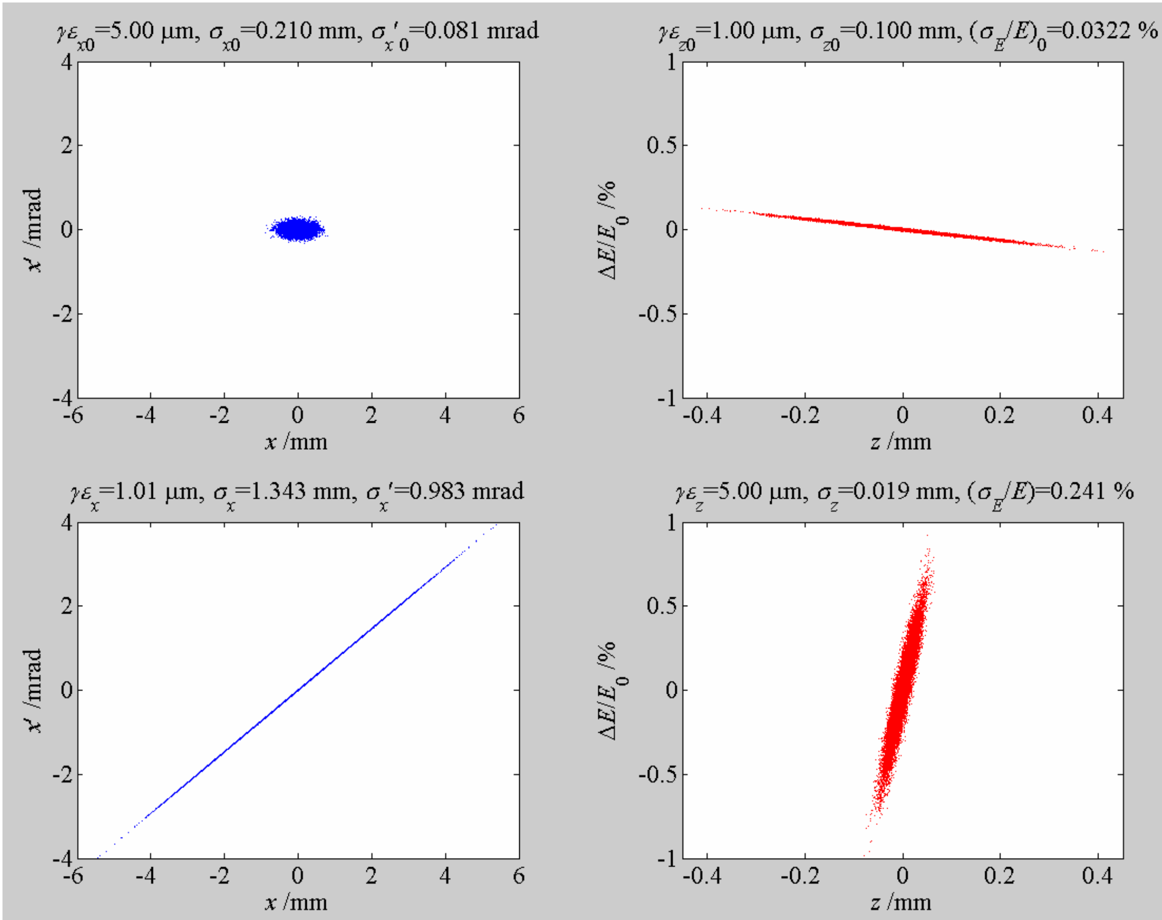

Figure 4. Initial (top) and final (bottom) phase space tracking plots with thick-lens cavity and α_z set according to (46). The emittances are still completely exchanged.

7 Applications

We have shown that, under appropriate conditions, it is possible to transfer the transverse emittance into the longitudinal plane, and the reverse. In a practical design, two systems might be used, one chicane-cavity system to reduce the horizontal emittance, and the other might be a similar concept, but using skew quadrupoles rather than the chicane-cavity system, to produce equal x and y emittances by exchanging some of the larger ε_y into the smaller ε_x. Two chicane-cavity systems, the second rotated by 90°, will not work because the first one increases the z-emittance above the transverse goal, and therefore inhibits the next y-emittance exchange.

The advantages of the emittance transfer scheme proposed here are a reduced dependence on the photoinjector to meet the transverse emittance goals, thus adding a considerable safety margin to the design. The chicane also compresses the bunch by acting on the amplified betatron oscillations of the RF-cavity, thereby adding another useful function to the scheme. The compression takes place entirely in the last bend. Coherent synchrotron radiation or longitudinal wakefields in the first two bends may present a severe limitation if the energy spread is increased significantly. Vacuum chamber shielding or low charge levels may be necessary depending on bend magnet and beam parameters. An additional bonus is that the reduction of the transverse emittance is accompanied by an increase of the local energy spread, a desirable requisite for the control of the CSR micro-bunching instability. Finally, the system allows a degree of control over bunch length, energy spread, and emittance and may add to the flexibility in manipulating electron beam parameters.

8 Acknowledgements

We would like to thank W. Spence for introducing us to many of the analytical methods employed in this treatment, and M. Woodley for help in running the *TURTLE* tracking. In addition we thank K. Bane, A. Chao, J. Irwin, A. Kabel, and G. Stupakov, for encouragement and useful comments. Prepared for the Department of Energy under contract number DE-AC03-76SF00515 by Stanford Linear Accelerator Center, Stanford University, Stanford, California, 94309, USA.

9 References

[1] "Linac Coherent Light Source (LCLS) Conceptual Design Report", SLAC-R-593, April 2002.

[2] S. Heifets, S. Krinsky, G. Stupakov, "CSR Instability in a Bunch Compressor", SLAC-PUB-9165, March 2002.

[3] E.L. Saldin, E.A. Schneidmiller, M.V. Yurkov, "Longitudinal Phase Space Distortions in Magnetic Bunch Compressors", 23rd International Free Electron Laser Conf. (FEL-2001), Darmstadt, Germany, August 2001.

[4] Z. Huang, K.-J. Kim, "Formulae for CSR Microbunching in a Bunch Compressor Chicane", submitted to *Phys. Rev. Spec. Topics – Acc. and Beams*, April 2002.

[5] H.G. Hereward, "Transverse Variation of Accelerating Force", CERN 58-12, June 1958.

[6] K.W. Robinson, "Radiation Effects in Circular Electron Accelerators", The Physical Review, Vol. 111, No. 2, p. 373, 1958.

[7] M. Cornacchia and A. Hofmann, "Radiation Damping Partitions and RF Fields", Proceedings of the 1995 Particle Accelerator Conference, Dallas, Texas, May 1-5, 1995.

[8] H. Okamoto, A. Sessler, D. Mohl, "Three-dimensional Laser Cooling of Stored and Circulating Ion Beams by Means of a Coupling Cavity", Phys. Rev. Letters, Vol. 72, No. 25, June 1994.

[9] A.M. Sessler and D.H. Whittum, "Radio-Frequency Beam Conditioner for Fast-Wave Free-Electron Generators of Coherent Radiation", Phys. Rev. Letters, Vol. 68, No. 3, January 1992.

[10] The matrix treatment used in this paper to describe the coupled x-z motion follows closely the unpublished work developed by W. Spence and P. Emma to describe the horizontally-vertically coupled motion in the collider arcs of the Stanford Linear Collider (1991).

[11] K.L. Brown, "Beam Envelope Matching for Beam Guidance Systems", SLAC-PUB-2370, August 1980.

[12] K.L. Brown, R.V. Servranckx, "Cross-Plane Coupling and its Effect on Projected Emittance", SLAC-PUB-4679, August 1989.

[13] Note that **S** is written here for a coordinate system with bunch head located at $z > 0$. If z is chosen with bunch head at $z < 0$, then $-\mathbf{J}$ should be used in the lower right block of **S**.

[14] D.C. Carey et al., "DECAY TURTLE: A Computer Program for Simulating Charged Particle Beam Transport Systems", SLAC-246, March 1982.